



UNIVERSITY OF LEEDS

This is a repository copy of *Dissecting Multivalent Lectin-Carbohydrate Recognition Using Polyvalent Multifunctional Glycan-Quantum Dots*.

White Rose Research Online URL for this paper:
<http://eprints.whiterose.ac.uk/119958/>

Version: Accepted Version

Article:

Guo, Y, Nehlmeier, I, Poole, E et al. (12 more authors) (2017) Dissecting Multivalent Lectin-Carbohydrate Recognition Using Polyvalent Multifunctional Glycan-Quantum Dots. *Journal of the American Chemical Society*, 139 (34). pp. 11833-11844. ISSN 0002-7863

<https://doi.org/10.1021/jacs.7b05104>

© 2017 American Chemical Society. This document is the Accepted Manuscript version of a Published Work that appeared in final form in *Journal of the American Chemical Society*, copyright © American Chemical Society after peer review and technical editing by the publisher. To access the final edited and published work see <https://doi.org/10.1021/jacs.7b05104>. Uploaded in accordance with the publisher's self-archiving policy.

Reuse

Items deposited in White Rose Research Online are protected by copyright, with all rights reserved unless indicated otherwise. They may be downloaded and/or printed for private study, or other acts as permitted by national copyright laws. The publisher or other rights holders may allow further reproduction and re-use of the full text version. This is indicated by the licence information on the White Rose Research Online record for the item.

Takedown

If you consider content in White Rose Research Online to be in breach of UK law, please notify us by emailing eprints@whiterose.ac.uk including the URL of the record and the reason for the withdrawal request.



eprints@whiterose.ac.uk
<https://eprints.whiterose.ac.uk/>

Dissecting Multivalent Lectin-Carbohydrate Recognition Using Polyvalent Multifunctional Glycan-Quantum Dots

Yuan Guo, Inga Nehlmeier, Emma Poole, Chadamas Sakonsinsiri, Nicole Hondow, Andy Brown, Qing Li, Shuang Li, Jessie Whitworth, Zhongjun Li, Anchi Yu, Rik Brydson, W. Bruce Turnbull, Stefan Pöhlmann, and Dejian Zhou

J. Am. Chem. Soc., **Just Accepted Manuscript** • DOI: 10.1021/jacs.7b05104 • Publication Date (Web): 08 Aug 2017

Downloaded from <http://pubs.acs.org> on August 10, 2017

Just Accepted

“Just Accepted” manuscripts have been peer-reviewed and accepted for publication. They are posted online prior to technical editing, formatting for publication and author proofing. The American Chemical Society provides “Just Accepted” as a free service to the research community to expedite the dissemination of scientific material as soon as possible after acceptance. “Just Accepted” manuscripts appear in full in PDF format accompanied by an HTML abstract. “Just Accepted” manuscripts have been fully peer reviewed, but should not be considered the official version of record. They are accessible to all readers and citable by the Digital Object Identifier (DOI®). “Just Accepted” is an optional service offered to authors. Therefore, the “Just Accepted” Web site may not include all articles that will be published in the journal. After a manuscript is technically edited and formatted, it will be removed from the “Just Accepted” Web site and published as an ASAP article. Note that technical editing may introduce minor changes to the manuscript text and/or graphics which could affect content, and all legal disclaimers and ethical guidelines that apply to the journal pertain. ACS cannot be held responsible for errors or consequences arising from the use of information contained in these “Just Accepted” manuscripts.

Dissecting Multivalent Lectin-Carbohydrate Recognition Using Polyvalent Multifunctional Glycan-Quantum Dots

Yuan Guo^{†,*}, Inga Nehlmeier[‡], Emma Poole[†], Chadamas Sakonsinsiri^{†,1}, Nicole Hondow[♠], Andy Brown,[♠] Qing Li[§], Shuang Li[¶], Jessie Whitworth[†], Zhongjun Li[§], Anchi Yu[¶], Rik Brydson[♠], W. Bruce Turnbull[†], Stefan Pöhlmann[‡], and Dejian Zhou^{†,*}

[†] School of Chemistry and Astbury Centre for Structural Molecular Biology, University of Leeds, Leeds LS2 9JT, United Kingdom.

[‡] Infection Biology Unit, German Primate Center, Kellnerweg 4, 37077 Gottingen, Germany.

[♠] School of Chemical and Process Engineering, University of Leeds, Leeds LS2 9JT, UK.

[§] Department of Chemical Biology, Peking University Health Sciences Centre, Beijing 100191, P.R. China.

[¶] Department of Chemistry, Renmin University of China, Beijing 100872, P.R. China.

¹ Current Address: Department of Biochemistry, Faculty of Medicine, Khon Kaen University, Khon Kaen 40002, Thailand.

Keywords: Quantum dot, DC-SIGN, multivalency, multi-modal readout, glyconanoparticle, virus inhibition, Förster resonance energy transfer

Abstract

Multivalent protein-carbohydrate interactions initiate the first contacts between virus/bacteria and target cells which ultimately lead to infection. Understanding the structures and binding modes involved is vital to the design of specific, potent multivalent inhibitors. However, the lack of structural information on such flexible, complex and multimeric cell surface membrane proteins has often hampered such endeavours. Herein we report that quantum dots (QDs) displayed with a dense array of mono-/di-saccharides are powerful probes for multivalent protein-glycan interactions. Using a pair of closely related tetrameric lectins, DC-SIGN and DC-SIGNR, which bind to the HIV and Ebola virus glycoproteins (EBOV-GP) to augment viral entry and infect target cells, we show that such QDs efficiently dissect the different DC-SIGN/R-glycan binding modes (tetra-/di-/mono- valent) through a combination of multi-modal readouts: Förster resonance energy transfer (FRET), hydrodynamic size measurement and transmission electron microscopy imaging. We also report a new QD-FRET method for quantifying QD-DC-SIGN/R binding affinity, revealing that DC-SIGN binds to the QD >100 fold tighter than DC-SIGNR. This result is consistent with DC-SIGN's higher trans-infection efficiency of some HIV strains over DC-SIGNR. Finally, we show that the QDs potently inhibit DC-SIGN-mediated enhancement of EBOV-GP-driven transduction of target cells with IC_{50} values down to 0.7 nM, matching well to their DC-SIGN binding constant (apparent $K_d = 0.6$ nM) measured by FRET. These results suggest that the glycan-QDs are powerful multifunctional probes for dissecting multivalent protein-ligand recognition and predicting glyconanoparticle inhibition of virus infection at the cellular level.

Introduction

Multivalent protein-carbohydrate interactions are widespread in biology and play a central role in many important biological events, including viral and bacterial infection, cell-cell communication and host immune response regulation.¹⁻⁵ Such interactions initiate the first contact between pathogens (*e.g.* viruses and bacteria) and target cells that ultimately leads to infection. However, monovalent protein-glycan interactions are intrinsically weak, and hence biologically inactive. To compensate this limitation, pathogens display arrays of specific glycans on their surface, allowing them to bind efficiently to multimeric glycan-binding proteins (lectins) on target cell surfaces and to exploit multivalency to enhance binding affinity and gain cell entry which ultimately lead to infection.³⁻⁶ Therefore, these multivalent interactions are attractive targets for developing novel antiviral interventions, especially entry inhibitors which can minimize virus resistance development.^{1-5,7} In this regard, the spatial- and orientation- match between the viral surface glycans and carbohydrate recognition domains (CRDs) of cell surface lectins is key to enhance binding affinity and specificity.^{8,9} Therefore, understanding the structure and spatial arrangement of the multivalent binding partners is essential for antiviral intervention which has been of focus of significant current research.^{1-5,7,10}

Synthetic glycoconjugates can block pathogen-lectin interactions whose inhibitory potency critically depends on the spatial- and orientation- match between the multivalent binding partners.^{3,8-14} However, a major challenge is the lack of structural information for many cell surface multimeric lectins, due to the problems associated with solving the structure of such flexible, complex and multimeric membrane proteins by X-ray crystallography. For example, despite extensive research over the past two decades, the complete crystal structures of two important pathogen receptors, the tetrameric dendritic cell receptor, DC-SIGN,¹⁵⁻²⁰ and its closely related endothelial cell receptor DC-SIGNR²¹ (collectively abbreviated as DC-SIGN/R hereafter), remain unknown apart from a structure model built upon the solution X-ray scattering data.²⁰ These two receptors play a key role in promoting HIV/Ebola virus (EBOV) infection

1
2
3
4
5 by binding to multiple mannose-containing glycans on the virus surface.^{15,18,19,21-23} Interestingly, despite
6
7 sharing 77% amino acid identity, an overall tetrameric structure,^{24,25} and identical individual CRD-
8
9 mannose binding motifs,¹⁷ these two receptors can differentially augment viral infectivity. For example,
10
11 DC-SIGN is more effective in augmenting the infectivity of some HIV strains than DC-SIGNR,^{18,23} while
12
13 only DC-SIGNR, but not DC-SIGN, can effectively promote West Nile virus infection.²⁶ Given their
14
15 close similarity, such differences must result from their different multivalent binding properties, arising
16
17 presumably from the different spatial and orientation arrangements of their four CRDs which have been
18
19 shown to be flexibly linked to the neck domain.²⁷ These observations make DC-SIGN/R an ideal pair of
20
21 model multimeric proteins to investigate how subtle structural differences influence multivalent protein-
22
23 glycan interactions. Unfortunately, the widely used biophysical techniques (*e.g.* isothermal titration
24
25 calorimetry (ITC)^{28,29} and surface plasmon resonance (SPR)³⁰), although powerful in providing
26
27 quantitative binding affinities, kinetics, and thermodynamics, cannot reveal the structural information
28
29 (e.g. binding mode, binding site distance and orientation) which is key to the design of potent multivalent
30
31 inhibitors.^{1,8,9,11} Therefore, there appear to be a clear capability gap of current methods in dissecting such
32
33 multivalent lectin-glycan interactions.
34
35
36
37
38

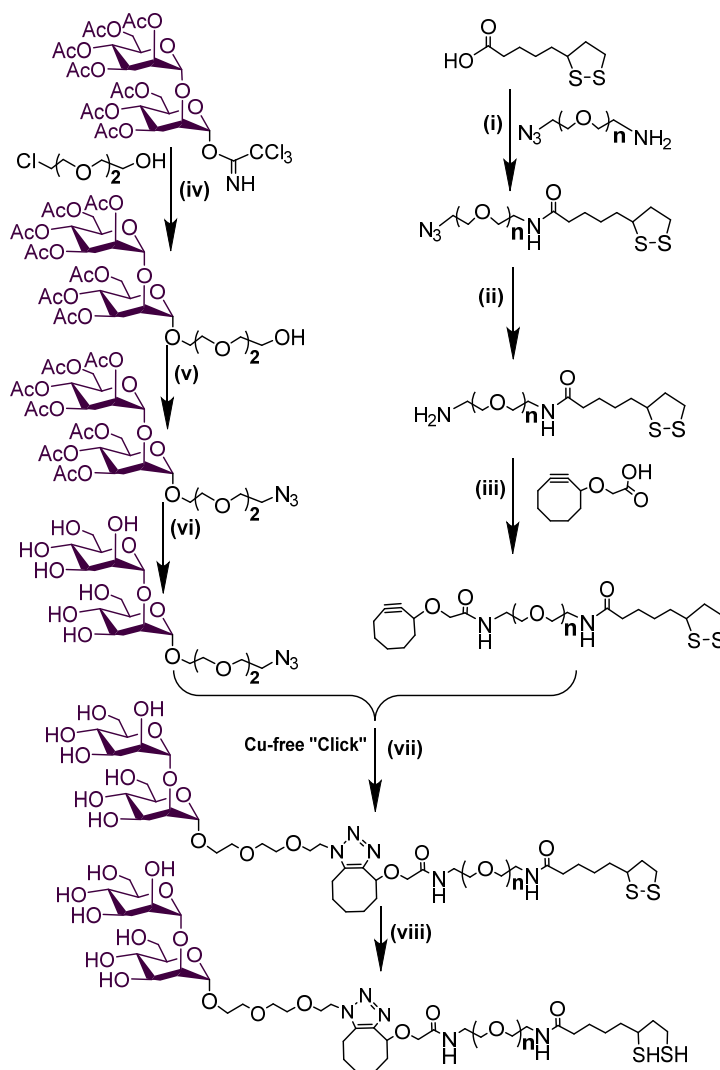
39
40 Herein we propose that this capability gap may be addressed by developing a polyvalent glycan-quantum
41
42 dot (QD-glycan)-based multimodal readout strategy to fully exploit multivalency and QD's unique
43
44 properties. First, the QD's unique, size-dependent, strong and stable fluorescence³¹⁻³³ can be harnessed
45
46 for binding quantification *via* a Förster resonance energy transfer (FRET) based ratiometric readout.³⁴⁻³⁸
47
48 Compared to other methods (*e.g.* SPR and ITC), the QD-FRET readout has the advantages of rapid,
49
50 separation-free detection in solution, high sensitivity, and a ratiometric readout signal with self-
51
52 calibration function, making it much less sensitive to instrument noise and signal fluctuation, allowing
53
54 for highly robust, accurate detection.³⁴⁻³⁷ Indeed, the QD-FRET technique has been widely employed to
55
56 address broad biological and biomedical problems, e.g. bio-/enzymatic-/intracellular- sensing, immuno-
57
58
59
60

1
2
3
4
5 assays, cell monitoring and tracking,³¹⁻⁴⁶ and more recently to probe multivalent protein-glycan
6
7 interactions.⁴⁷ Second, the solid nanoscale core of the QD can be decorated with polyvalent specific
8
9 glycan ligands to enhance binding affinity by exploiting multivalency. Third, the QD-protein binding
10
11 can be directly monitored in solution by dynamic light scattering *via* binding induced hydrodynamic size
12
13 changes. Finally, the high contrast of the QD core in scanning transmission electron microscopy (STEM)
14
15 can be harnessed to directly visualize binding-induced particle arrangements so as to probe the exact
16
17 binding mode. Despite extensive research, most QD-FRET work reported so far have only utilized the
18
19 fluorescence property of the QD, hence the unique multi-functionality of the QD probe has not been fully
20
21 exploited. For example, using the QD-FRET readout strategy, we have recently found that compact
22
23 polyvalent mono-mannose-capped QDs (QD-Man) specifically bind to DC-SIGN, but not to DC-SIGNR.
24
25 We have also proposed that the four CRDs face upwards in DC-SIGN, but point sideways in DC-SIGNR,
26
27 making the latter unable to bind multivalently (>2) to one QD.⁴⁷ However, QD-Man failed to differentiate
28
29 binding of DC-SIGNR and monovalent CRD (SI, Figure S1),⁴⁷ possibly due to the fact that the individual
30
31 CRD-mannose binding is too weak to measure at low concentrations. Therefore, the overall QD-Man-
32
33 DC-SIGN/R binding modes remain unclear. Herein we solved this problem by increasing the individual
34
35 CRD binding affinity of the glycan displayed on the QD and by developing a novel multimodal readout
36
37 strategy comprising FRET, hydrodynamic size measurement and S/TEM imaging to fully exploit the
38
39 unique multi-functionality of the glycan-QD. We further show that there is a good correlation between
40
41 the QDs' DC-SIGN/R binding affinity and their virus inhibition potency.
42
43
44
45
46
47
48
49

50 Results and Discussion

51
52 **Glycan ligand design and synthesis.** To increase individual CRD-glycan binding affinity, manno-
53
54 pyranosyl- α -1,2-manno-pyranose (DiMan) was coupled to the terminal end of the dihydrolipoic acid-
55
56 oligo(ethylene glycol)- based multifunctional ligands^{48,49} (abbreviated as DHLA-EG_n-DiMan hereafter,
57
58 where n = 3 or 11 stands for a uniform linker containing 3 or 11 EG units, respectively) using the route
59
60

described in Scheme 1. For comparison, their mono-mannosyl equivalent ligands (*e.g.* DHLA-EG_n-Man, n = 3 or 11) were also synthesised as described previously.⁴⁷ Individual DiMan-CRD binding is ~4 times as strong as that of Man-CRD (*K_d* ~0.9 versus 3.5 mM),²⁹ allowing us to investigate how individual CRD-glycan affinity contributes to the overall QD-glycan-DC-SIGN/R multivalent binding.



Scheme 1. The synthetic route to DHLA-EG_n-DiMan (where n = 3 or 11). Reaction conditions were: (i) DCC/DMAP, DCM; (ii) triphenyl-phosphine, EtOAc/H₂O; (iii) DCC/DMAP, DCM; (iv) BF₃.OEt₂, DCM, molecular sieves, (v) NaN₃/TBAI, DMF; (vi) NaOMe, MeOH, then Amberlite H⁺ resin; (vii) EtOH; (viii) TCEP.HCl, CHCl₃/EtOH/H₂O.

1
2
3
4
5 Briefly, Lipoic acid (LA) was first coupled to $\text{NH}_2\text{-EG}_n\text{-N}_3$ ($n = 3, 11$) to form $\text{LA-EG}_n\text{-N}_3$ (step i). It was
6
7 then reduced to $\text{LA-EG}_n\text{-NH}_2$ by triphenyl-phosphine (step ii), and then coupled to cyclooctyne-COOH
8
9 to form $\text{LA-EG}_n\text{-cyclooctyne}$ (step iii). Meanwhile, 3,4,6-tri-*O*-acetyl-2-*O*-(2,3,4,6-tetra-*O*-acetyl- α -D-
10
11 mannopyranosyl)- α -D-mannopyranosyl-trichloroacetimidate was reacted with 2-[2-(2-chloroethoxy)
12
13 ethoxy]ethanol to introduce a EG_2 linker (step iv), which was then treated with NaN_3 to convert the linker
14
15 terminal hydroxyl group into an azide (step v), after removal of the acetyl protection groups, the azide
16
17 modified glycan, (1-azido-3,6-dioxaoct-8-yl-2-*O*- α -D-manno-pyranosyl- α -D-mannopyranoside), was
18
19 obtained (step vi). After that, the azide modified glycan was coupled to $\text{LA-EG}_n\text{-cyclooctyne}$ *via* the Cu-
20
21 free “click” chemistry to give $\text{LA-EG}_n\text{-glycan}$ (step vii), and reduction by tris(2-carboxyethyl)phosphine
22
23 (TCEP) gave the desired final DHLA- $\text{EG}_n\text{-Glycan}$ ligand. Details of the synthesis procedures and their
24
25 spectroscopic data are given in the Supporting Information (SI). Each DHLA- $\text{EG}_n\text{-glycan}$ ligand contains
26
27 three different functional domains: a DHLA for robust chelative QD capping;^{48,50} a hydrophilic, flexible
28
29 EG_n linker for imposing high water-solubility, stability and resistance against non-specific adsorption as
30
31 well as for tuning the inter-sugar spacing; and a terminal glycan for specific protein binding.⁴⁷
32
33
34
35
36
37

38 **Preparation and characterization of glycan-QDs.** The DHLA- $\text{EG}_n\text{-glycan}$ ligands, after deprotonation
39
40 by NaOH, were directly used to initiate cap-exchange with a commercial hydrophobic CdSe/ZnS QD
41
42 ($\lambda_{\text{EM}} \sim 560$ nm) in a homogenous solution using our recently developed highly efficient cap-exchange
43
44 method.⁴⁷ Details of the cap-exchange procedures were given in the SI, part 3. All of the resulting DHLA-
45
46 $\text{EG}_n\text{-glycan}$ capped QDs (abbreviated as QD- $\text{EG}_n\text{-glycan}$ hereafter) formed highly stable dispersions in
47
48 aqueous media, and displayed no noticeable changes in appearance or fluorescence over times >1 month.
49
50 Moreover, the QDs were compact and uniform in size, displaying a small hydrodynamic diameter (D_h)
51
52 of 8.3 and 9.5 nm for QD- $\text{EG}_3\text{-DiMan}$ and QD- $\text{EG}_{11}\text{-DiMan}$, respectively (Figure S2),⁵¹ suggesting the
53
54 formation of isolated, aggregation-free QD dispersions.⁵²⁻⁵⁵ Importantly, the QDs were densely capped
55
56 with the glycan ligands (glycan valency >220), which would be difficult to achieve by other methods
57
58
59
60

(e.g. post cap-exchange chemical coupling). Using the D_h values and corresponding glycan valencies, the average inter-glycan distances (d) of the QD-EG_n-glycans were estimated in the range of 0.9-1.3 nm (Table 1, see SI Section 6.1 for calculation method). Interestingly, this distance matches well to the average inter-glycan sequon distance (~1.2 nm) found on the HIV surface heavily glycosylated glycoprotein, gp120.^{56,57} Moreover, the QD surface glycan density and inter-glycan distance (d) can be readily tuned by varying the linker length and diluting the DHLA-EG_n-glycan ligand using an inert hydrophilic spacer ligand, DHLA-zwitterion, during the cap-exchange process (see Figure 1).

Table 1. Summary of the chemical and physical parameters of the QD-EG_n-glycan conjugates.

QD surface Ligands	Glycan valency	D_h (nm)	Inter-glycan spacing (nm)	Glycan footprint on QD surface (nm ²)
DHLA-EG ₃ -Man	330±70	8.9±0.1	0.98±0.11	0.75±0.16
DHLA-EG ₁₁ -Man	222±62	9.6±0.2	1.29±0.36	1.30 ±0.36
DHLA-EG ₃ -DiMan	369±38	8.3±0.1	0.86±0.09	0.59 ± 0.06
DHLA-EG ₁₁ -DiMan	281±25	9.5±0.1	1.13±0.10	1.01±0.09

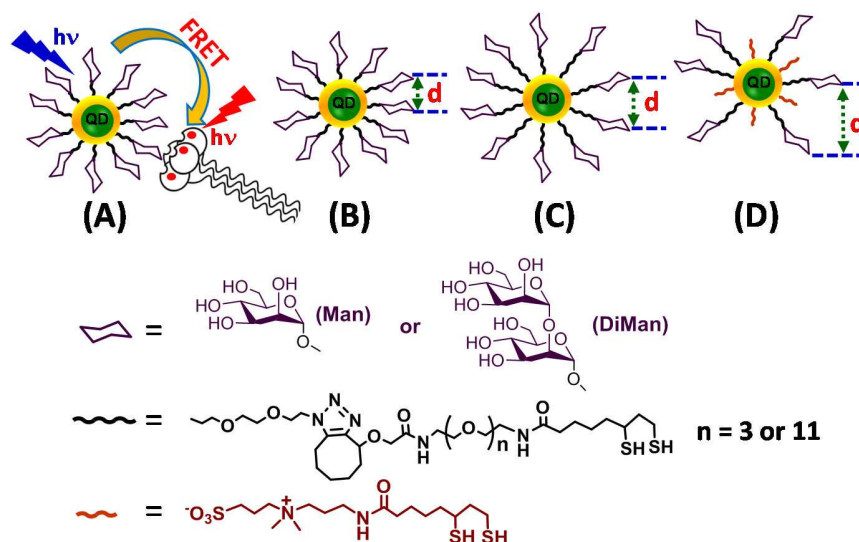


Figure 1. (A) Schematic showing our approach to quantify QD-glycan-DC-SIGN/R multivalent binding by QD-sensitized dye FRET mechanism. (B, C, D) Schematic presentation of tuning the QD surface glycan valency and inter-glycan distance (d) via EG linker length ($n = 3$ for B; $n = 11$ for C) and glycan dilution with an inert DHLA-zwitterion spacer ligand (D).

1
2
3
4
5 **Differentiating QD-DiMan-DC-SIGN/R binding modes by FRET.** The DC-SIGN/R proteins were
6
7 expressed and labeled with an Atto-594 dye at a site-specifically introduced cysteine residue on the CRD
8
9 (SI part 4).⁴⁷ The chosen mutation residue (Q274 in DC-SIGN and R287 in DC-SIGNR) is located out
10
11 with the glycan binding sites, minimizing any possible interference with CRD glycan binding. The QD
12
13 emission has good overlap with the Atto-594 absorption, ensuring that efficient FRET can occur (Förster
14
15 radius $R_0 = \sim 4.0$ nm, Figure S3), but has minimal overlap of dye emission spectra, allowing for easy
16
17 separation of the QD and dye FRET signal without the need of spectral deconvolution. We first screened
18
19 the QD-glycan-DC-SIGN/R binding by titrating different amounts of labeled proteins into a fixed
20
21 concentration of the QD-glycan (40 nM) in a binding buffer (20 mM HEPES, 100 mM NaCl, 10 mM
22
23 CaCl₂, pH 7.8). The resulting fluorescence spectra were shown in Figure 2 (all spectra have been
24
25 corrected by dye direct excitation background). Similar to QD-Man, incubation of QD-DiMan with the
26
27 labeled DC-SIGN resulted in significant quenching of QD fluorescence ($\lambda_{EM} \sim 554$ nm) and an concurrent
28
29 enhancement of the Atto-594 FRET signal ($\lambda_{EM} \sim 626$ nm), consistent with a QD-sensitized Atto-594
30
31 FRET mechanism (Figure 2). Moreover, the FRET signal was found to be strongly Ca²⁺-dependent and
32
33 was completely diminished in the absence of Ca²⁺ (SI, Figure S4). This observation is fully consistent
34
35 with the Ca²⁺-dependency of the DC-SIGN-glycan binding.^{17,24} Despite such similarities, three major
36
37 differences between QD- DiMan and QD-Man binding to DC-SIGN/R were observed:
38
39
40
41
42
43
44

45 (1) Most significantly, binding of DC-SIGNR to QD-DiMan produced notable FRET signals which were
46
47 markedly higher and well-separated from those of the monovalent CRDs (Figure 2 and SI, Figure S5), a
48
49 sharp contrast to that of QD-Man where signals obtained from DC-SIGNR and monovalent CRD binding
50
51 were equally weak and indistinguishable from non-specific adsorption background (SI, Figure S1).⁴⁷
52
53 Moreover, the apparent FRET ratios (I_{626}/I_{554}) obtained from the monovalent CRD-QD-DiMan binding
54
55 were still indistinguishable from the background, suggesting that monovalent binding is too weak (K_d
56
57 ~ 0.9 mM)²⁹ to measure with 40 nM QD. Given that the I_{626}/I_{554} ratio is linearly correlated to the number
58
59
60

of acceptors (proteins) bound to each QD in the absence of other quenching effect (see SI, section 5.5),⁴⁷ this result implies that DC-SIGNR-QD-DiMan binding is multivalent, and not monovalent, otherwise similar FRET ratios would have been expected.

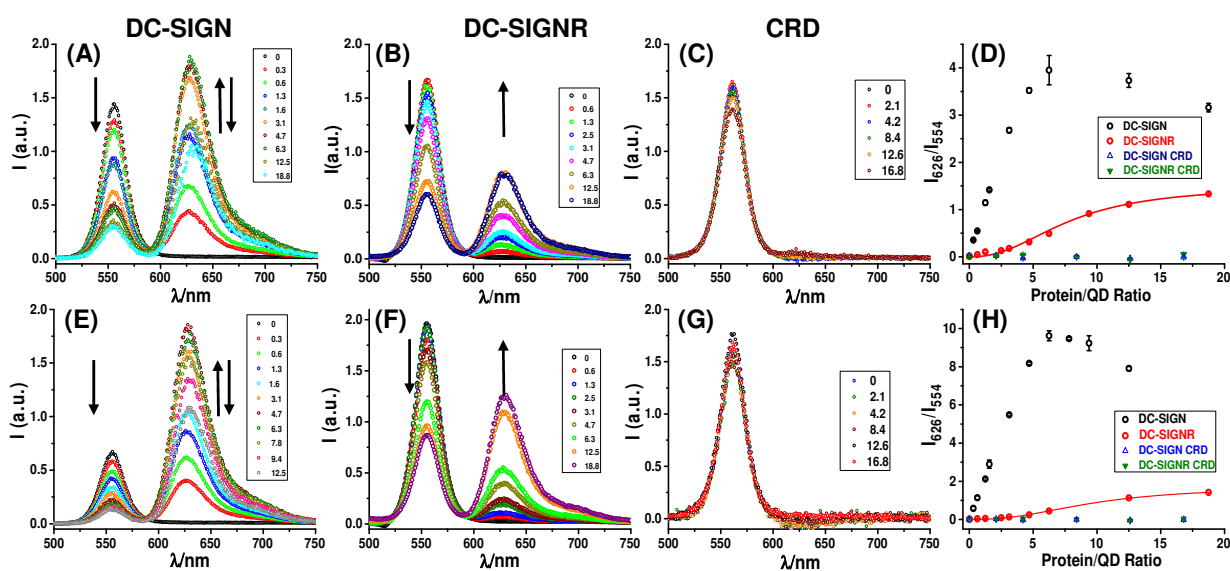


Figure 2. Dye-direct excitation background-corrected fluorescence spectra of QD-DiMan (100% glycan density) after binding to Atto-594-labeled proteins at different protein:QD ratios (PQR): QD-EG₁₁-DiMan + DC-SIGN (A); QD-EG₁₁-DiMan + DC-SIGNR (B); QD-EG₁₁-DiMan + DC-SIGN CRD (C); QD-EG₃-DiMan + DC-SIGN (E); QD-EG₃-DiMan + DC-SIGNR (F), QD-EG₃-DiMan + DC-SIGN CRD (G), and the resulting I_{626}/I_{554} ratio *v.s.* PQR relationship for QD-EG₁₁-DiMan (D) and QD-EG₃-DiMan (H). DC-SIGNR binding data are fitted by Hill's equation, $y = R_{max} \times x^n / (k^n + x^n)$, where R_{max} is the maximum I_{626}/I_{554} ratio, k is the PQR value that gives 50% R_{max} , and n is the Hill coefficient. The best fit parameters are $R_{max} = 2.6 \pm 0.9$, $k = 17.2 \pm 6.1$, $n = 1.5 \pm 0.1$ and $R^2 = 0.9984$ for QD-EG₁₁-DiMan and $R_{max} = 1.7 \pm 0.2$, $k = 9.7 \pm 1.5$, $n = 2.4 \pm 0.4$ and $R^2 = 0.9991$ for QD-EG₃-DiMan.

(2) Binding of DC-SIGN to QD-DiMan still produced a much stronger FRET signal than that of DC-SIGNR (Figure 2), suggesting that DC-SIGN must display a higher binding multivalency to one QD than DC-SIGNR. These results are not unexpected, and in fact, they are fully consistent with our proposed QD-DC-SIGN/R binding models.⁴⁷ The four side-way facing CRDs in DC-SIGNR may split into two pairs and bind divalently with two different QDs. This binding mode should result in positive binding

1
2
3
4
5 cooperativity. Fitting the DC-SIGNR binding curves by the Hill's function: $y = R_{max} \times x^n / (k^n + x^n)$, where
6
7 R_{max} is the maximum I_{626}/I_{554} ratio, k is the protein:QD ratio (PQR) that gives 50% R_{max} , and n is the Hill
8
9 coefficient, indeed revealed that the n for both QD-EG₁₁-DiMan (1.5 ± 0.1) and QD-EG₃-DiMan (2.4 ± 0.4)
10
11 were > 1 , clearly confirming positive binding cooperatively (Figure 2D/2H). In contrast, the four
12
13 upwardly facing CRDs in DC-SIGN may bind tetravalently to a single QD which should produce no
14
15 binding cooperativity ($n \leq 1$). Indeed, a similar Hill's fit of the DC-SIGN binding curves with QD-DiMan
16
17 with 25% glycan density revealed the n to be 0.85 ± 0.15 for QD-EG₁₁-DiMan and 1.0 ± 0.3 for QD-EG₃-
18
19 DiMan, confirming no binding cooperativity (Figure 3). Here the QD surface glycan density used in DC-
20
21 SIGN binding was diluted to 25% by DHLA-zwitterion ligand to avoid FRET quenching observed with
22
23 100% glycan density QDs at high PQRs (see Figure 2D/2H and the next section). Therefore, the different
24
25 binding multivalency modes of DC-SIGN/R have been successfully differentiated *via* polyvalent QD-
26
27 DiMan binding and a ratiometric FRET readout strategy.

28
29
30
31
32
33 (3) Interestingly, unlike the QD-Man-DC-SIGN binding, where the apparent FRET ratio (I_{626}/I_{554})
34
35 followed a typical binding pattern with increasing PQR before reaching saturation (Figure S1), the QD-
36
37 DiMan-DC-SIGN interaction exhibited a distinct two-stage response (Figure 2I/J). The I_{626}/I_{554} ratio
38
39 initially increased roughly linearly with the PQR at < 6 as expected for a single QD-donor in a FRET
40
41 interaction with N identical receptors model; however, the I_{626}/I_{554} ratio then decreased with the
42
43 increasing PQR at > 6 . Using the surface areas calculated from the D_h s of the QDs and the DC-SIGN
44
45 head footprint, the number of DC-SIGN molecules that can be packed onto the QD surface without
46
47 crowding was estimated as $\sim 6/\sim 8$ for QD-EG₃-DiMan/QD-EG₁₁-DiMan, respectively (Figure S6). These
48
49 numbers approximately match the critical PQR (the turning point on the FRET response curve),
50
51 suggesting that surface crowding is responsible for the observed FRET decrease. The quenching is likely
52
53 due to crowding-induced reorganisation of the QD-bound DC-SIGNs *via* their flexible neck region²⁷ that
54
55 brings the dyes in proximity to each other and causes mutual quenching. This assignment was supported
56
57
58
59
60

by that no quenching was observed for the labeled DC-SIGN only under equivalent concentrations in the absence of QD-DiMan (Figure S7). Consistent with these results, the fluorescence lifetime of the QD-EG₁₁-DiMan (14.75 ns) was reduced to 7.75 ns and further to 1.76 ns as PQR increased from 3 to 10. Meanwhile, the dye lifetime (3.48 ns for protein only) was increased to 8.09 ns at PQR = 3, but then decreased to 4.00 ns at PQR = 10 (Figure S8).⁵⁸ Interestingly, diluting the QD surface DHLA-EG_n-glycan density to 25% with DHLA-ZW removed the two stage behaviour and the binding curves returned to their normal shape without FRET quenching at high PQRs (Figure 3C/3F). However, it also produced significantly lower (~4 fold) FRET ratios at saturation (Figure 3C/3F), suggesting a significantly reduced DC-SIGN binding capacity for the 25% glycan-QD. This result further supports the proposal of surface crowding induced CRD reorganisation being responsible for the FRET quenching observed with the 100% glycan-QDs under high PQRs.

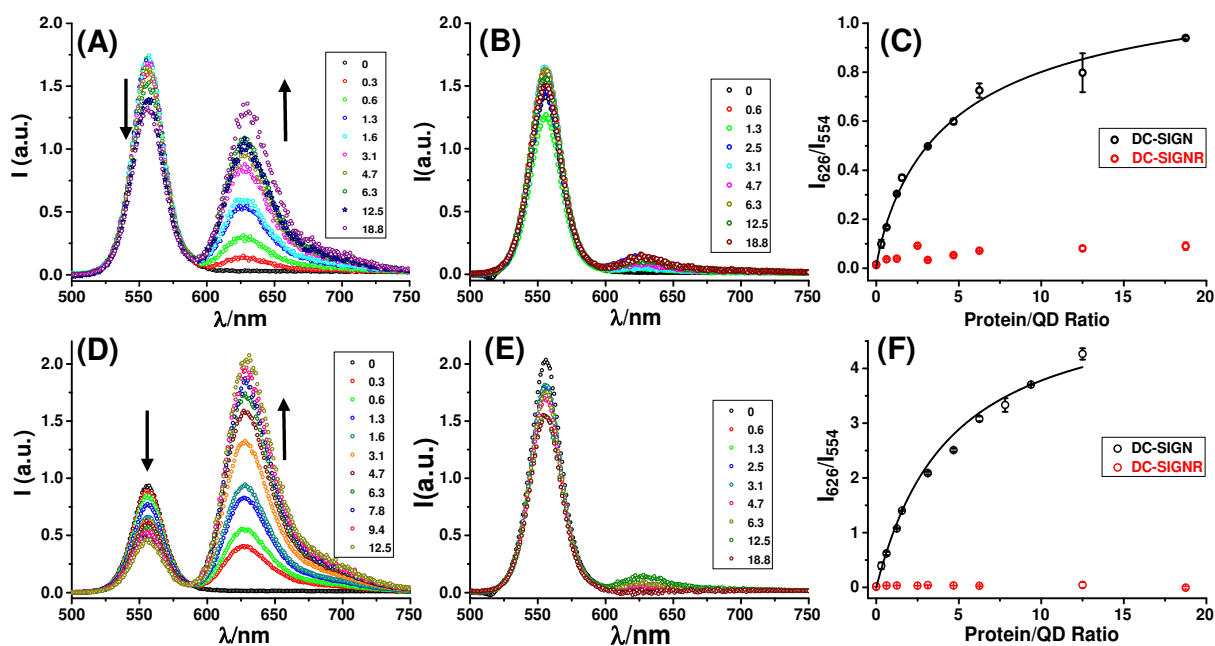


Figure 3. Dye-direct excitation background-corrected fluorescence spectra of QD-EG_n-DiMan (with 25% glycan density diluted by DHLA-ZW ligands) after binding to Atto-594-labeled proteins at different PQRs: QD-EG₁₁-DiMan + DC-SIGN (A); QD-EG₁₁-DiMan + DC-SIGNR (B); QD-EG₃-DiMan + DC-SIGN (D); QD-EG₃-DiMan + DC-SIGNR (E) and the I_{626}/I_{554} ratio *v.s.* PQR relationship for QD-EG₁₁-

1
2
3
4
5 DiMan (C) and QD-EG₃-DiMan (F). The DC-SIGN binding data were fitted to the Hill's equation, giving
6 $R_{max} = 1.2 \pm 0.2$, $k = 4.9 \pm 2.1$, $n = 0.85 \pm 0.15$, and $R^2 = 0.9918$ for QD-EG₁₁-DiMan and $R_{max} = 5.4 \pm 1.6$, k
7 $= 4.4 \pm 3.1$, $n = 1.0 \pm 0.3$, and $R^2 = 0.9994$ for QD-EG₃-DiMan.
8
9

10
11
12
13
14 Using the FRET efficiency obtained from the QD quenching (*e.g.* $E = I - I/I_0$, where I and I_0 are the
15 fluorescence intensities of the QD with and without the protein, respectively) and a single QD in FRET
16 interaction with N identical acceptor model, $E = I/[I + (r/R_0)^6/N]$,³⁴ the average QD-dye distance r was
17 calculated to be ~ 5.2 and ~ 5.7 nm for DC-SIGN binding to QD-EG₃-DiMan and QD-EG₁₁-DiMan,
18 respectively (SI, Figure S3C & D). Both r values were ~ 1 nm longer than the hydrodynamic radii of the
19 corresponding QD-EG_{*n*}-glycans (*e.g.* ~ 4.2 and ~ 4.8 nm). This result is not unreasonable considering the
20 distance between the dye labeling position and the glycan binding site, as well as the flexible nature of
21 the EG_{*n*} linker which may become more extended upon protein binding. However, the equivalent FRET
22 efficiency *v.s.* dye:QD ratio responses for DC-SIGNR binding to QD-DiMan were S-shaped and could
23 not be fitted by the single QD in FRET interaction with N identical acceptor model (SI, Figure S3C/D).
24 The relatively weak binding between DC-SIGNR and QD-DiMan (>100 fold weaker than that of DC-
25 SIGN equivalent, see the next section) and positive binding cooperatively may have led to the S-shape
26 response curve: presumably because DC-SIGNR added under low PQRs was unable to bind efficiently
27 to QD-DiMan to produce efficient FRET at the early stages of titration.
28
29
30
31
32
33
34
35
36
37
38
39
40
41
42
43
44
45

46 **Quantifying QD-glycan-DC-SIGN/R binding affinity by FRET.** The different QD-binding modes and
47 multivalency exhibited by DC-SIGN/R should result in differing binding affinities (K_{dS}). Theoretically,
48 the I_{626}/I_{554} ratio is linearly correlated to the numbers of acceptors (proteins) bound to the QD, making it
49 a reliable signal for quantifying the proportion of the bound QD-protein complexes in a QD/protein
50 mixture (SI part 5.4).^{47,59} Here we have developed a new method by simultaneously changing the
51 QD/protein concentration whilst keeping PQR fixed at 1 for DC-SIGN (to avoid the FRET quenching at
52
53
54
55
56
57
58
59
60

high PQRs) or 10 for DC-SIGNR (to compensate the low FRET ratio at $PQR = 1$, Figure S9). Under such conditions, the I_{626}/I_{554} intensity ratio can provide a true reflection of the fraction of bound QD-protein complexes within the QD-protein mixture. The experiments were performed in the binding buffer containing 1 mg/ml of bovine serum albumin (BSA) to minimise the possible non-specific adsorption of QD/protein on surfaces which were non-negligible at low concentrations (<10 nM).⁵⁹ The resulting fluorescence spectra revealed that both the dye FRET and QD fluorescence signals increased with the increasing concentration (SI, Figure S9). However, the former increased faster than the latter, giving an increased I_{626}/I_{554} ratio with the increasing concentration. The resulting I_{626}/I_{554} ratio-concentration relationships were fitted by the Hill's equation to derive the apparent dissociation constants (K_{ds} , Figure 4). The parameters derived from the best fits were summarized in Table 2.

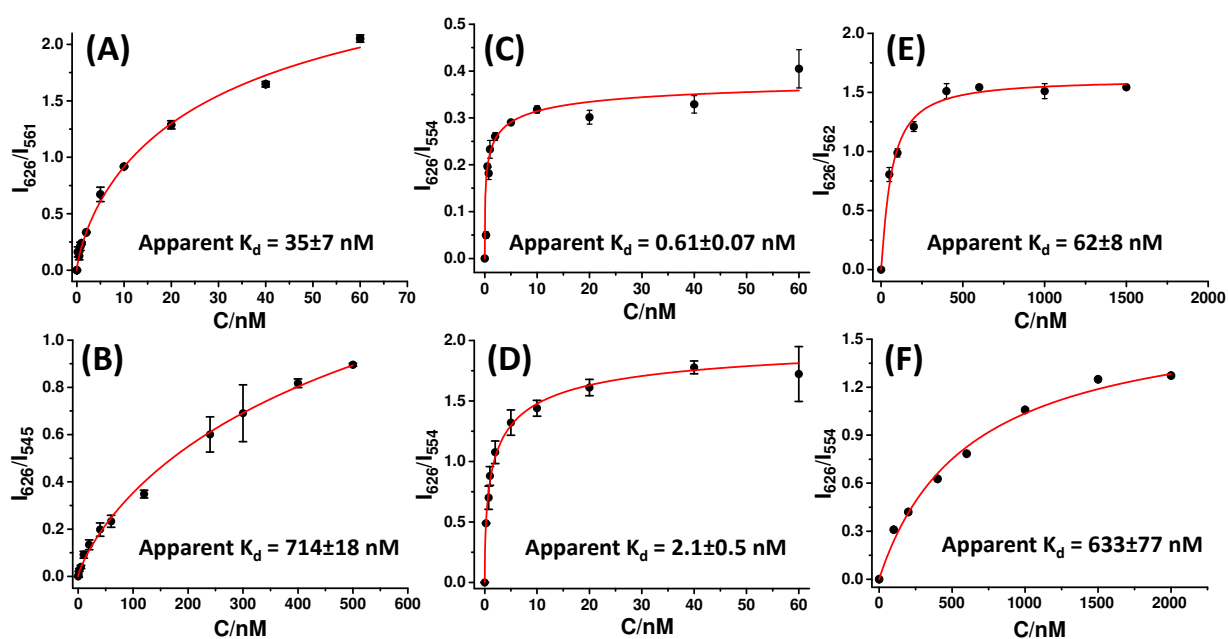


Figure 4. Relationship between the I_{626}/I_{554} ratio and protein concentration for a fixed protein:QD molar ratio of 1:1 for DC-SIGN and 10:1 for DC-SIGNR. (A): DC-SIGN + QD-EG₃-Man; (B) DC-SIGN + QD-EG₁₁-Man; (C) DC-SIGN + QD-EG₃-DiMan; (D) DC-SIGN + QD-EG₁₁-DiMan; (E) DC-SIGNR + QD-EG₃-DiMan; and (F) DC-SIGNR + QD-EG₁₁-DiMan. Data were fitted by the Hill's equation, $Y =$

$R_{max} \times C^n / [K_d^n + C^n]$, where R_{max} , K_d , n and C are the maximum I₆₂₆/I₅₅₄ ratio, apparent K_d , Hill coefficient, and protein concentration, respectively. The fitting parameters were summarised in SI, Table S1.

Table 2. Key chemical and biophysical parameters of the QD-EG_n-glycans and their binding affinities with DC-SIGN/R measured by FRET.

QD Surface Ligands	Glycan valency (N)	Apparent K_d DC-SIGN (nM)	Apparent K_d DC-SIGNR (nM)	Enhancement factor β *	β/N
DHLA-EG ₃ -Man	330±70	35±7	/	100,000	~300
DHLA-EG ₁₁ -Man	222±62	714±18	/	4,900	~22
DHLA-EG ₃ -DiMan	369±38	0.61±0.07	62 ± 8	1,480,000	~4,000
DHLA-EG ₁₁ -DiMan	281±25	2.1±0.5	633±77	430,000	~1,500

* DC-SIGN affinity enhancement factor is calculated by: $\beta = K_d(\text{CRD-Glycan}) / \text{Apparent } K_d(\text{DC-SIGN-QD})$, where $K_d(\text{CRD-Man})$ and $K_d(\text{CRD-DiMan})$ are 3.5 and 0.9 mM, respectively.²⁹

Four notable findings are revealed by Table 2. First, a polyvalent display of DiMan on the QD greatly enhanced its affinity for DC-SIGN: a remarkably low apparent K_d of 610 pM was achieved with QD-EG₃-DiMan, translating to a massive ~1.5 million fold affinity enhancement (β) over the monovalent CRD-DiMan binding ($K_d \sim 0.9$ mM),²⁹ and a normalised per sugar enhancement factor, β/N , of ~4000. Second, although a polyvalent display of Man on the QD also enhanced its DC-SIGN affinity, the level of enhancement was significantly lower than that of the DiMan equivalent (< 1/10 in β/N terms). This difference may be due to the extended binding surface of the DC-SIGN CRD which contains both primary and secondary binding sites.^{17,24} For QD-Man, it may bind mainly to the primary site whereas QD-DiMan may bind to both primary and secondary sites, leading to greater affinity enhancement. Third, the apparent K_d for QD-DiMan binding to DC-SIGN was found to be >100 fold lower than that to DC-SIGNR, suggesting that DC-SIGN's binding affinity is >100 fold stronger than that of DC-SIGNR. Given that each HIV surface gp120 trimer spike is densely coated with mannose containing glycans⁵⁷ and is of

1
2
3
4
5 comparable size (~12 nm)⁶⁰ to a QD-DiMan, this result thus provides a plausible explanation why DC-
6
7 SIGN has been found to be more effective in trans-infecting some HIV strains than DC-SIGNR.²³
8
9 Moreover, this result explains the reason why wild-type DC-SIGNR was unable to compete off DC-
10
11 SIGN from binding to QD-DiMan observed in the next section. Finally, the flexible EG linker also had
12
13 a significant impact on the overall binding affinity: increasing the linker length from 3 to 11 EG units led
14
15 to >3 fold lower affinity. This is presumably because the longer the EG linker the more flexible and
16
17 disordered the terminal glycans will be, hence there is a greater entropic penalty to pay upon DC-SIGN
18
19 binding. Nevertheless, a suitable EG linker is essential to impose high QD stability in aqueous media and
20
21 to minimise non-specific interactions with non-target proteins.
22
23
24
25

26 **Confirming QD-DC-SIGN/R binding specificity using wild-type receptor competition.** A FRET
27
28 competition experiment using unlabeled wild-type proteins was further employed to confirm that the
29
30 labeled DC-SIGN/R (containing a site-specific cysteine mutation and Atto-594 labeling, see SI, section
31
32 4)-QD binding truly reflected wild-type protein binding properties. The experiment was performed on
33
34 the QDs with 25% glycan density to overcome the FRET quenching problem observed with 100%
35
36 glycan-QD (Figure S10A). As wild-type protein:labeled DC-SIGN ratio (WLR) increased, the FRET
37
38 signal reduced progressively while the QD fluorescence correspondingly recovered (Figure 5A),
39
40 confirming that wild-type DC-SIGN successfully displaced labeled DC-SIGNs from binding to the QD.
41
42 In contrast, wild-type DC-SIGNR caused no apparent changes to either the QD or the FRET signal
43
44 (Figure 4B), suggesting no binding competition occurred. These results indicate that wild-type and
45
46 labeled DC-SIGN molecules must bind to the same sugar sites (same binding mode) on the QD surface,
47
48 whereas DC-SIGNR may be too weak to displace the labeled DC-SIGN from binding to the QD. Their
49
50 different competition efficiencies were clearer in the normalised I_{626}/I_{554} versus WLR plots (Figure 4C),
51
52 where DC-SIGNR gave no apparent changes but DC-SIGN yielded significantly reduced FRET ratios.
53
54
55
56
57
58
59
60

This result is not unexpected because DC-SIGNR-QD-DiMan binding is >100 fold weaker than that of the equivalent DC-SIGN interaction (see previous section, Table 2).

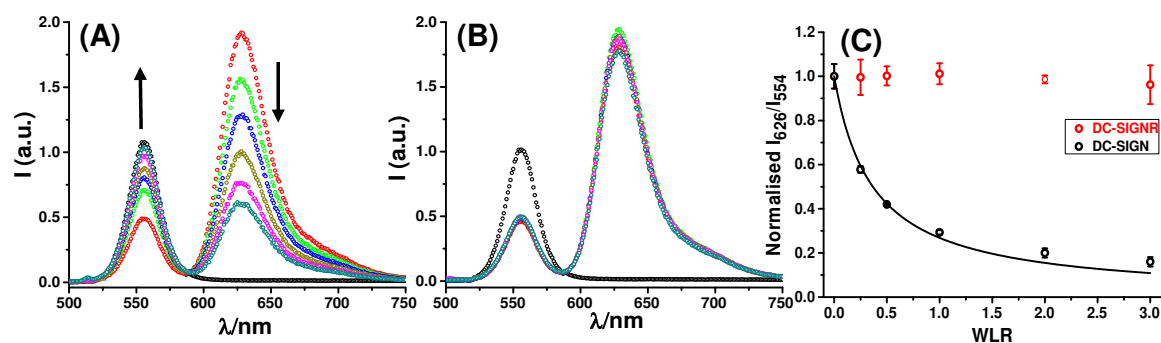


Figure 5. Dye-direct excitation background corrected fluorescence spectra of QD-EG₃-DiMan(25%)/DHLA-ZW(75%) + Atto-594 labeled DC-SIGN (PQR = 12.5 to ensure saturate protein binding) after mixing with different amounts of wild-type DC-SIGN (A) or DC-SIGNR (B). The QD-only fluorescence spectra in the absence of proteins are also displayed for comparison (shown in black open circles). (C) Plots of the corresponding normalized I_{626}/I_{554} ratio *versus* wild-type protein:labeled DC-SIGN molar ratio (WLR) fitted by a competitive binding model.

The relative affinity between wild-type and labeled DC-SIGN for the QD-DiMan binding was further evaluated by a simple competitive model, $F = IR_{50}/[IR_{50} + C_{WT}/C_{LP}]$, where F is the FRET ratio in the presence of wild-type protein normalised by that without, C_{WT} and C_{LP} are wild-type and labeled protein concentrations, respectively, and IR_{50} is the molar ratio of wild type DC-SIGN:labeled DC-SIGN required to reduce F by 50%. An IR_{50} value of 1 indicates that both proteins bind to the QD with equal affinity, while an IR_{50} value of < 1 indicates that the labeled protein binds more weakly than wild-type protein. Fitting the data using this model gave an IR_{50} value of 0.88 and 0.37 for QD-EG₁₁-DiMan and QD-EG₃-DiMan, respectively (Figure 5, and SI, Figure S10). Both IR_{50} values were <1, indicating that the site-specific mutation and dye-labeling in DC-SIGN weakened its binding affinity with the QDs. This

effect was more pronounced for QD-EG₃-DiMan, presumably because its shorter EG₃ linker may limit the terminal sugar's ability to re-organise and fit perfectly within the protein's binding pockets.

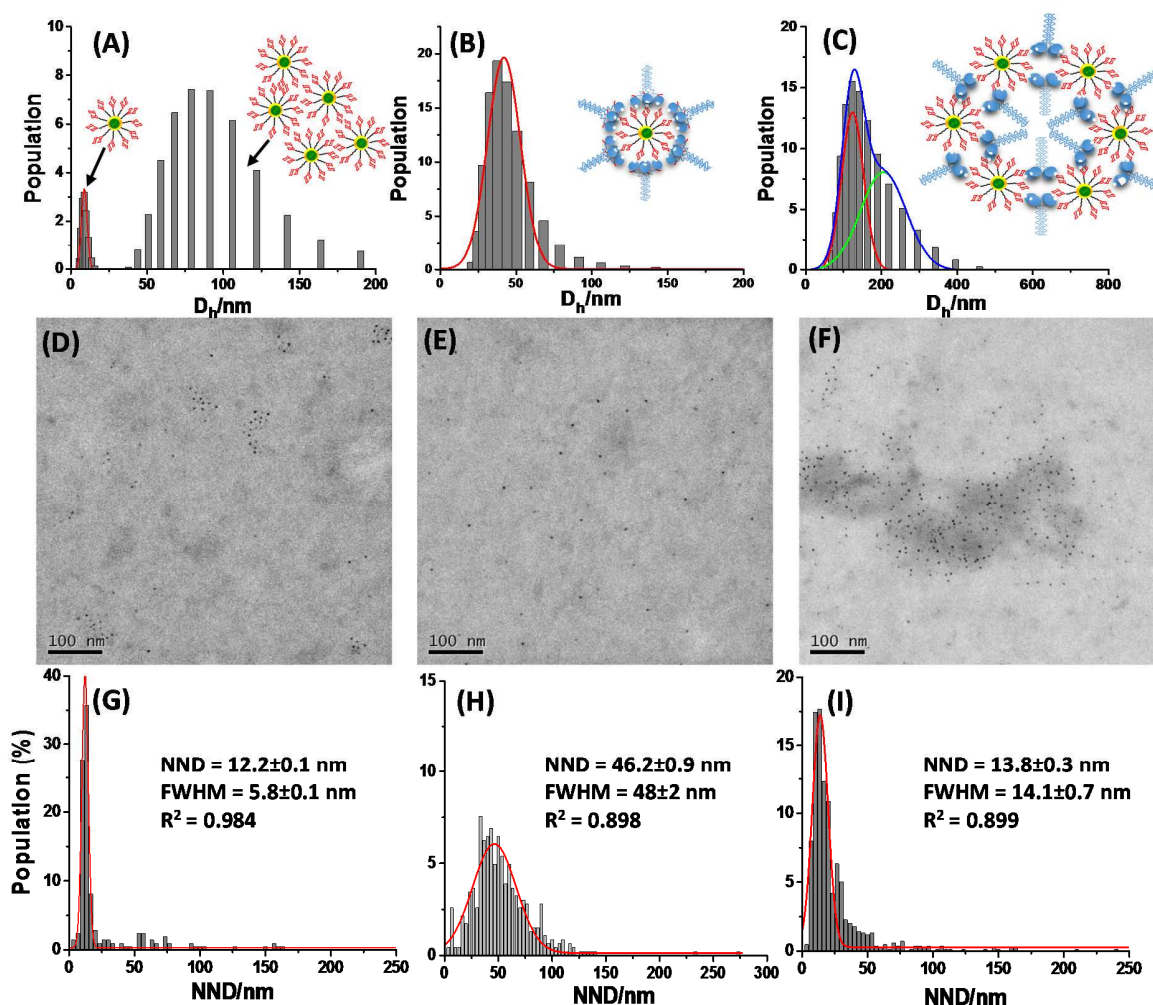


Figure 6. Hydrodynamic diameter histograms of QD-EG₁₁-DiMan before (A) and after binding to wild-type DC-SIGN (B) or DC-SIGNR (C) measured by dynamic light scattering (DLS). Insets show schematics of the QD and/or QD-protein assemblies. Cryo-TEM (contrast inverted HAADF STEM) images of the QD-EG₁₁-DiMan before (D) and after binding to wild-type DC-SIGN (E) or DC-SIGNR (F). Consistent with the D_h values shown in (A), both isolated and clustered QDs are found in the corresponding TEM image (D) for QD-EG₁₁-DiMan. Histograms of nearest neighbour distance (NND) distributions measured from the TEM images of QD-EG₁₁-DiMan before (G) and after binding to wild-type DC-SIGN (H) or DC-SIGNR (I). The distribution histograms were fitted by Gaussian function with fitting parameters shown in each graph. All samples were measured in binding buffer.

Differentiating QD-wild type protein binding modes by DLS, TEM and fluorescence quenching.

The hydrodynamic size (D_h) of the QD-protein assemblies provided further support for the different binding modes of DC-SIGN/R.⁵¹ Binding of wild-type DC-SIGN with QD-EG₁₁-DiMan (PQR = 12.5) gave only a single, narrowly distributed species with a D_h of ~42 nm (Figure 6B). This value was significantly bigger than that of isolated QDs (D_h ~ 8.8 nm in binding buffer, Figure 6A) or wild-type DC-SIGN (D_h ~14 nm, Figure S11), suggesting that all DC-SIGNs were bound to the QD and formed a uniform QD-protein assembly. In contrast, binding of wild-type DC-SIGNR gave a bimodal distribution with D_h s of *ca.* 124 and 205 nm (Figure 6C), respectively. Moreover, almost identical D_h distributions were also observed with its equivalent QD-EG₃-DiMan interaction (SI, Figure S2D, Table S2). These D_h values were too large to be isolated individual QD-protein assemblies, a strong indication of QD agglomeration *via* QD/DC-SIGNR inter-linking. This hypothesis was confirmed by two dimensional imaging of the QD dispersions *via* rapid plunge freezing and subsequent TEM/STEM imaging at low magnification after analytical confirmation of the QD size and contrast level in these images⁶¹ (we term this cryo-snapshot TEM/STEM, SI, part 6), where the high contrast of the QD was employed as the differentiating modality. Figure 6D shows that the QDs clustered in the binding buffer, possibly due to weak binding between Ca²⁺ ions and QD-surface DiMan ligands since QD-DiMan appeared as isolated particles in pure water without Ca²⁺ (Figure S12). However, the QD-DiMan clusters were completely dispersed upon binding with wild-type DC-SIGN, revealing only isolated QDs (Figure 6E); whereas binding of wild-type DC-SIGNR produced more aggregated QDs (Figure 6F). The different binding behaviours were further supported by a nearest neighbour particle distance (NND) analysis of TEM images (see SI, part 6).⁶¹ A large NND of ~46 nm was found for DC-SIGN bound QDs, which was >3 times that of DC-SIGNR bound QDs (~14 nm) or clustered QDs in binding buffer (~12 nm, see Figure 6G/H/I). These results agree excellently with the DLS results and our proposed DC-SIGN/R binding

1
2
3
4
5 modes. The strong tetravalent binding of DC-SIGN with one QD should produce isolated QDs,
6
7 preventing them from getting close to each other and hence a large NND; whereas the bis-divalent
8
9 binding of DC-SIGNR with two different QDs should lead to QD inter-linking and a small NND.

10
11
12 The postulated DC-SIGN/R-QD binding modes were further supported by the different fluorescence
13
14 quenching behaviors by DHLA-EG₃-DiMan coated gold nanoparticles (GNP-EG₃-DiMan, Figure S13).
15
16 GNP was chosen here because its efficient universal fluorescence quenching can extend beyond the
17
18 traditional FRET distance limit of ~10 nm.^{62,63} Here a 605 nm emitting QD was used to minimise the QD
19
20 fluorescence reduction due to absorption of GNP at the excitation wavelength ($\lambda_{EX} = 590$ nm). Mixing
21
22 GNP-EG₃-DiMan (5 nM) with QD-EG₃-DiMan (10 nM) in binding buffer gave almost the same
23
24 fluorescence as the QD alone, suggesting minimal QD-GNP cross-linking. Addition of wild-type DC-
25
26 SIGNR to the QD-GNP mixture significantly quenched the QD fluorescence, whereas introduction of
27
28 wild-type DC-SIGN increased the QD fluorescence considerably (Figure S14). These results matched
29
30 well to that expected from the DC-SIGN/R binding modes: cross-linking by DC-SIGNR should lead to
31
32 QD/GNP assembly and QD fluorescence quenching by the proximal GNPs; whereas the strong
33
34 tetravalent binding of DC-SIGN to one QD or GNP should not only prevent any GNP or QD assembly,
35
36 but also break up any pre-assembled QD clusters in binding buffer (see Figure 6D), resulting in higher
37
38 fluorescence over the QD-only sample
39
40
41
42
43
44

45 **Inhibiting DC-SIGN/R-mediated augmentation of EBOV-GP-driven viral entry.** The strong DC-
46
47 SIGN binding affinity afforded by QD-EG_n-DiMan suggests that these QDs could effectively block DC-
48
49 SIGN-mediated virus infection. To investigate this potential, a murine leukemia virus (MLV)-based
50
51 vector bearing the EBOV-GP was employed to deliver the luciferase gene into human embryonic kidney
52
53 cells (293T) previously transfected to express DC-SIGN/R.⁴⁷ The virus particles can bind to cell surface
54
55 DC-SIGN/R *via* incorporated EBOV-GPs on their membrane surface to enhance cell uptake and gene
56
57 transduction. As expected, DC-SIGN/R expression in cells greatly increased the efficiency of EBOV-
58
59
60

GP-driven gene transduction. Pre-treatment of cells with QD-EG_n-DiMan greatly reduced the gene transduction of DC-SIGN-positive cells down to the low nM range, indicating high inhibition potency (Figure S15). The normalised inhibition data were fitted by an inhibition model, giving an IC₅₀ of 0.7±0.2 and 1.4±0.1 nM for QD-EG₃-DiMan and QD-EG₁₁-DiMan, respectively (Figure 7). Such low IC₅₀ values place them among the most potent glyconanoparticle inhibitors against EBOV-GP-driven transduction of host cells. In fact, their inhibition potency is comparable to the giant globular multivalent glycofullerenes (IC₅₀ = 0.667 nM)¹⁴ and the virus-like glycodendri-nanoparticles (IC₅₀ = 0.91 nM).¹³

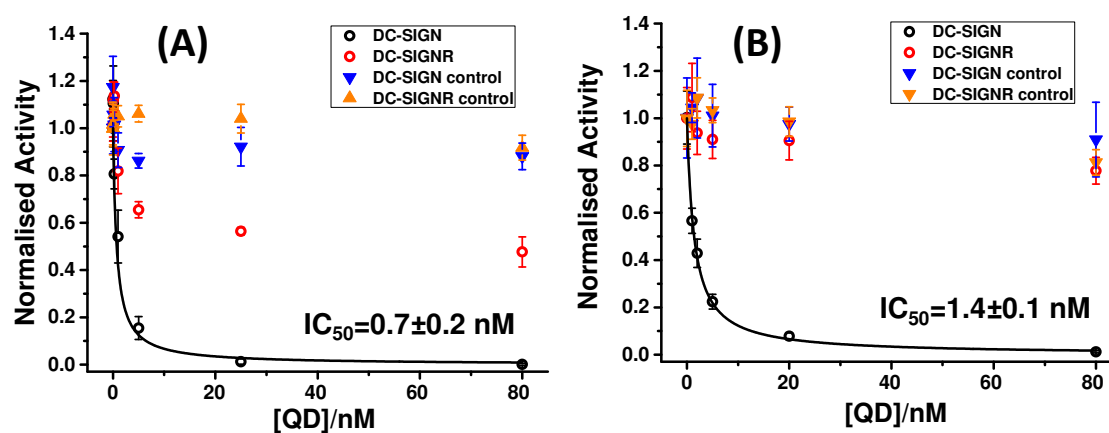


Figure 7. Normalised luciferase activities of the DC-SIGN- or DC-SIGNR- expressing 293T cells as a function of the pre-treatment QD-EG₃-DiMan (A) or QD-EG₁₁-DiMan (B) concentration. The data for particles bearing the Ebola virus glycoprotein (EBOV-GP) are shown in open circles while the results obtained with control particles bearing the vesicular stomatitis virus glycoprotein (VSV-G) are shown in triangles. The luciferase activities, after subtraction by their corresponding pcDNA control background, were normalised by the respective values in the absence of the QDs (SI, Figure S15). Data were fitted by a competitive binding model, $F = IC_{50}/(IC_{50} + C_{QD})$, where F is the normalized luciferase activity, C_{QD} is the QD concentration, and IC_{50} is the concentration that gives 50% inhibition.⁴⁷ The gene transduction driven by a control vector bearing VSV-G, which cannot use DC-SIGN/R to augment cell entry, was unaffected by the QD treatment, confirming that the specific QD-DC-SIGN/R binding was responsible for the observed inhibition.

1
2
3
4
5 Interestingly, these IC_{50} values roughly matched their apparent binding K_{dS} with DC-SIGN (*i.e.* 0.61 and
6
7 2.1 nM) measured by QD-FRET (Table 2). Moreover, the gene transduction of DC-SIGNR-expressing
8
9 cells was reduced only marginally by treatment with 80 nM QD-EG₁₁-DiMan (~10%) but it was more
10
11 pronounced with QD-EG₃-DiMan (~50%). The inhibition potencies obtained here again roughly matched
12
13 those expected from their respective DC-SIGNR binding apparent K_{dS} (*i.e.* ~633 and ~62 nM) measured
14
15 by FRET. The good match between the apparent K_d and IC_{50} values demonstrated that our FRET based
16
17 K_d measurement could serve as a viable, rapid method for predicting virus inhibition potency of
18
19 glyconanoparticles at the cellular level. Although the toxic cadmium content can prevent the current QD-
20
21 glycans from being used for treatment and prevention of EBOV infection, replacing the CdSe/ZnS QD
22
23 with other biocompatible, non-toxic nanoparticles (*e.g.* gold, Cd-free QD) should overcome this problem,
24
25 where nanoparticles displayed with similar polyvalent glycan ligands could be used as potent, specific
26
27 virus inhibitors and therapeutic reagents.
28
29
30
31
32

33 Conclusions

34
35 We have demonstrated that compact QDs displaying dense polyvalent DHLA-EG_n-DiMan ligands are
36
37 powerful probes for dissecting multivalent protein-glycan interactions *via* multimodal readout strategies
38
39 (FRET, particle size analysis, TEM imaging and GNP-based fluorescence quenching). Unlike most other
40
41 glycoconjugates which were constructed on passive scaffolds, the unique properties of QD (*e.g.*
42
43 fluorescence, size and inherent TEM contrast) have been fully exploited for the purpose of multimodal
44
45 readout for the first time. Significantly, we have revealed that DC-SIGN binds tetravalently to a single
46
47 QD, whereas DC-SIGNR binds divalently to two different QDs. The different binding modes, arising
48
49 from the different CRD spatial arrangements, yields >100 fold tighter QD-DiMan binding affinity for
50
51 DC-SIGN over DC-SIGNR which also help to explain why DC-SIGN is more effective in trans-infecting
52
53 some HIV strains than DC-SIGNR. Moreover, a new QD-FRET-based ratiometric method has been
54
55 developed to quantify the apparent QD-protein binding K_{dS} . An impressively low K_d (~610 pM) and a
56
57
58
59
60

1
2
3
4
5 per glycan affinity enhancement factor (β/N) of ~ 4000 have been attained with QD-DiMan. Importantly,
6
7 QD-DiMan was found to potently inhibit DC-SIGN-mediated augmentation of EBOV-GP-driven
8
9 infection of host cells with an IC_{50} of ~ 0.7 nM, placing it among the most potent inhibitors against the
10
11 EBOV-GP driven virus infections.^{10,13,14} Moreover, this IC_{50} value also matches well to its DC-SIGN
12
13 binding apparent K_d measured by the ratiometric QD-FRET readout strategy. Together, these results
14
15 demonstrate that the QD-FRET-based affinity measurement developed herein could serve as a robust,
16
17 rapid, and sensitive method for predicting glyconanoparticle inhibition potencies against EBOV-GP
18
19 driven virus infections at the cellular level.
20
21
22
23
24
25

26 **Experimental Section**

27 **Materials**

28
29
30
31 A CdSe/ZnS core/shell QD ($\lambda_{EM} \sim 560$ nm) was purchased from PlasmaChem GmbH (Berlin, Germany).
32
33 The QD was supplied as dry powders and capped with mixed ligands of trioctylphosphine oxide (TOPO),
34
35 hexadecylamine and oleic acid. A CdSe/ZnSe/ZnS core/shell/shell QD capped with mixed ligands of
36
37 TOPO and trioctylphosphine ($\lambda_{EM} \sim 605$ nm) in toluene was purchased from STREM chemicals UK Ltd.
38
39 O-(2-Aminoethyl)-O'-(2-azidoethyl)decylethylene glycol (N_3 -EG₁₁-NH₂, >95% oligomer purity) was
40
41 purchased from Polypure Plc (Norway). Azido-3,6,9-trioxyundecan-1-amine (N_3 -EG₃-NH₂, >90%
42
43 monomer purity), N,N-dimethyl-1,3-propanediamine (>99%), 1,3-propane-sultone (> 99%), liponic acid
44
45 (LA, >99%), triphenylphosphine (>98.5%), dicyclohexyl-carbodiimide (DCC, >99%), dimethylamino-
46
47 pyridine (DMAP, >99%), tris(2-carboxyethyl)phosphine hydrochloride (TCEP.HCl, >98%), and other
48
49 chemicals were purchased from Sigma-Aldrich UK Ltd (Dorset, UK). Solvents were obtained from
50
51 Fisher Scientific (Loughborough, UK). Ultra-pure water (resistance >18.2 M Ω .cm) purified by an ELGA
52
53 Purelab classic UVF system, was used for all experiments and making buffers.
54
55
56
57
58
59
60

1
2
3
4
5 **Preparation of QD-EG_n-glycan (n = 3 or 11).**⁴⁷ 1 nmol CdSe/ZnS QD in 0.2 mL toluene was first
6 precipitated by 1 mL ethanol followed by centrifugation to remove any free ligands. The QD pellet was
7 dissolved in CHCl₃ (50 μL), then DHLA-EG_n-glycan ligand (0.80 μmol in CHCl₃) pre-deprotonated by
8 NaOH (8.0 μL, 0.10 M in EtOH) and MeOH were added to make a homogenous solution (CHCl₃:MeOH
9 = 1:1 v/v). The resulting solution was wrapped in an aluminium foil and stirred at room temperature (RT)
10 for 30 min. Hexane was then added until the solution became cloudy. The mixture was centrifuged at
11 10,000 g for 5 min, where all the formed QD-EG_n-glycan pelleted. After removal of the clear supernatant,
12 the pellet was dissolved in 100 μL of pure H₂O and transferred to a 30 KDa MWCO spin column and
13 washed with H₂O (3 × 100 μL) to remove any unbound free ligands, yielding the QD-EG_n-glycan stock.
14 The QD concentration was determined by its first exciton peak absorbance at 546 nm ($\epsilon = 1.3 \times 10^5 \text{ M}^{-1} \text{ cm}^{-1}$)
15 using the Beer-Lambert law.⁴⁷
16
17
18
19
20
21
22
23
24
25
26
27
28
29
30

31 **Fluorescence spectroscopy.** All fluorescence spectra were recorded on a Cary Eclipse fluorometer using
32 a fixed excitation wavelength, λ_{EX} , of 450 nm, corresponding to the absorption minimum of Atto-594 to
33 minimise the direct excitation background. The measurements were performed in a binding buffer (20
34 mM HEPES pH 7.8, 100 mM NaCl, 10 mM CaCl₂) containing 10 μg/mL of a His₆-Cys peptide which
35 we found to improve the QD stability and reduce non-specific adsorption.^{47,59} The labeled proteins were
36 mixed with the QD at RT for 20 min before fluorescence spectra were recorded. Binding of labeled
37 monomeric DC-SIGN or DC-SIGNR CRD with the QDs was performed the same way. For apparent K_d
38 measurement, a series of samples containing different concentrations of the QD/labeled proteins (but
39 with a fixed PQR of 1 for DC-SIGN or 10 for DC-SIGNR) were prepared in the same binding buffer as
40 above but containing 1 mg/mL of BSA to reduce non-specific adsorption. The samples were incubated
41 at RT for 20 min before fluorescence spectra were recorded. Adjustments of the PMT voltages and
42 EX/EM slit widths were used to compensate the low fluorescence signal at low concentrations. Although
43 this may affect the absolute fluorescence intensity, the FRET ratio is not affected due to its ratiometric
44
45
46
47
48
49
50
51
52
53
54
55
56
57
58
59
60

1
2
3
4
5 nature. All fluorescence spectra were corrected for the dye direct excitation background by subtracting
6
7 the corresponding fluorescence spectrum of the same concentration labeled protein only recorded under
8
9 identical conditions.
10

11
12 **Data Fitting.** Direct excitation background corrected fluorescence peak intensities at 554 nm (QD) and
13
14 626 nm (Atto-594 FRET) were used to calculate the apparent FRET ratio, I_{626}/I_{554} . The I_{626}/I_{554} ratio
15
16 *versus* protein concentration plots were fitted to the Hill's equation to derive the apparent K_d :
17
18

$$I_{626}/I_{554} = (R_{\max} \times [C]^n) / (K_d^n + [C]^n) \quad (1)$$

19
20
21
22
23 Where R_{\max} is the saturated FRET ratio, K_d is the apparent dissociation constant, $[C]$ is the protein
24
25 concentration and n is Hill's coefficient. Iterative fittings were used to yield the best fit (R^2) for R_{\max} and
26
27 K_d determination. The relative binding affinity between wild-type and labeled DC-SIGN for the QD-
28
29 DiMan was analysed by a simple competitive model, $F = IR_{50} / [IR_{50} + C_{WT}/C_{LP}]$.
30
31

32
33
34 Where F is the apparent FRET ratio in the presence of wild-type protein normalised by that without, C_{WT}
35
36 and C_{LP} are wild-type and labeled protein concentrations, respectively. Iterative fittings were used to
37
38 yield the best fit (R^2) for the IR_{50} determination.
39
40

41 **STEM imaging.** Three QD samples (QD-EG11-DiMan, QD-EG11-DiMan + wild-type DC-SIGN and
42
43 QD-EG11-DiMan + wild-type DC-SIGNR) were prepared in binding buffer with $C_{QD} = 40$ nM and C_{protein}
44
45 = 1.5 μ M. 3.5 μ L of the QD sample was placed onto a plasma-cleaned TEM grid with a continuous
46
47 carbon support film, blotted, and plunge frozen into liquid ethane. The TEM grids were then warmed to
48
49 RT over several min by placing them in the liquid nitrogen cooled storage container in a rotary pumped
50
51 vacuum desiccator. The samples were analysed using an FEI Titan Cubed Themis 300 G2 S/TEM
52
53 equipped with FEI SuperX energy dispersive X-ray (EDX) spectrometers. The samples were imaged
54
55 using high angle annular dark field scanning transmission electron microscopy (HAADF STEM)
56
57 mode,^{61,64} which provides atomic number contrast ($\approx Z^{1.7}$), thereby permitting imaging of the high atomic
58
59
60

1
2
3
4
5 number quantum dots (brighter) on the low atomic number background (darker). A series of images at
6
7 the same magnification were recorded for each sample which were then analysed in MATLAB to
8
9 measure the nearest neighbour distances (NNDs). Histograms of NNDs for each image were produced.
10
11 The combined histograms were plotted as a percentage of the total population and fitted by Gaussian
12
13 distribution.
14

15
16
17 **Inhibition of DC-SIGN/R-mediated augmentation of EBOV-GP-driven transduction.**⁴⁷ The
18
19 experiments were performed using human embryonic kidney 293T cells. Target 293T cells seeded in 96-
20
21 well plates were transfected with plasmids encoding DC-SIGN or DC-SIGNR or control transfected with
22
23 empty plasmid (pcDNA). The cells were washed at 16 h post transfection and further cultivated at 37°C,
24
25 5% CO₂ in Dulbecco's modified eagle medium (DMEM) containing 10% fetal bovine serum (FBS). At
26
27 48 h post transfection, the cells were exposed to twice the final concentration of QD-DiMan inhibitor in
28
29 DMEM supplemented with 10% FBS for 30 min in a total volume of 50 µl. Thereafter, the cells were
30
31 inoculated with 50 µl of preparations of MLV vector particles encoding the luciferase gene and bearing
32
33 either EBOV-GP or the vesicular stomatitis virus glycoprotein (VSV-G) as control. Binding of QD-
34
35 DiMan to DC-SIGN/R on the surface of 293T cells can block the interaction of these lectins with the
36
37 EBOV-GP on the particle surface, reducing the cellular uptake of vector particles and thus reducing
38
39 transduction efficiency. At 6 h post inoculation, 100 µl of fresh DMEM culture medium was added and
40
41 the cells incubated for another 72 h. Thereafter, luciferase activities in cell lysates were determined using
42
43 a commercially kit (PJK), following the manufacturer's instructions, as described in our previous
44
45 publication.⁴⁷
46
47
48
49
50

51 52 53 54 55 **ASSOCIATED CONTENT**

56 57 **Supporting Information**

58
59
60

1
2
3
4
5 The Supporting Information is available free of charge on the ACS Publications website at
6
7 <http://pubs.acs.org>.
8

9
10 Experimental details which include the detailed synthesis and spectroscopic characterization of the
11
12 DHLA-EG_n-DiMan ligands, DC-SIGN/R production and labeling; lifetime measurement, STEM and
13
14 DLS measurements, calculation of inter-glycan distance, virus inhibition experiment, supporting tables
15
16 showing the physical parameters of the QD-EG_n-glycan, fitting parameters, and supporting figures
17
18 showing the hydrodynamic size distributions of the proteins and QDs with and without proteins; QD-
19
20 Atto594 Förster radius (R_0) and average QD-dye distance (r); Ca²⁺-dependence of DC-SIGN/R QD
21
22 binding; lifetime decay curves; GNP-DiMan hydrodynamic size and TEM image; QD fluorescence
23
24 quenching by GNP in the presence of DC-SIGN/R, and original virus inhibition data.
25
26
27
28
29

30 AUTHOR INFORMATION

31 Corresponding authors:

32
33 * Email: y.guo@leeds.ac.uk (Y.G.), fax: +44-113-3436565.
34
35

36
37 * Email: d.zhou@leeds.ac.uk (D.Z.), tel: +44-113-3436230; fax: +44-113-3436565.
38
39

40 ORCID

41
42 Yuan Guo: 0000-0003-4607-7356
43
44

45
46 Bruce Turnbull: 0000-0002-7352-0360
47
48

49
50 Stefan Pöhlmann: 0000-0001-6086-9136
51
52

53
54 Dejian Zhou: 0000-0003-3314-9242
55

56 Author Contributions

1
2
3
4
5 Y.G., D.Z., and S.P. conceived research. Y.G., I.N., E.P., C.S., N.H., Q.L., S.L., J.W. and A.B. performed
6 research. Y.G., D.Z., N.H., E.P., A.Y., S.P. and W.B.T. analysed data. D.Z. and Y.G. wrote the paper.
7
8 All authors have discussed the results and approved the final version of the paper.
9

10 11 Notes

12 The authors declare no competing financial interest.
13
14
15

16 17 ACKNOWLEDGMENTS

18
19 We thank the Wellcome Trust (Grant No: 097354/Z/11/Z), BBSRC (Grant No: BB/M005666/1) and the
20 University of Leeds for funding this project. Y.G. thanks the Wellcome Trust for supporting a career re-
21 entry fellowship (Grant No: 097354/Z/11/Z). E.P. thanks the University of Leeds and EPSRC for funding
22 her a DTA PhD studentship. C.S. thanks Khon Kaen University and its Faculty of Medicine for providing
23 a PhD studentship. We also thank Dr M. Rowan Brown (Swansea University, UK) for the development
24 of MATLAB scripts that enabled automation of nearest neighbour measurements in TEM images.
25
26
27
28
29
30

31 32 Reference

- 33 (1) Bhatia, S.; Camacho, L. C.; Haag, R. *J. Am. Chem. Soc.* **2016**, *138*, 8654.
34 (2) Mammen, M.; Choi, S. K.; Whitesides, G. M. *Angew. Chem. Int. Ed.* **1998**, *37*, 2755.
35 (3) Bernardi, A.; Jimenez-Barbero, J.; Casnati, A.; De Castro, C.; Darbre, T.; Fieschi, F.; Finne, J.;
36 Funken, H.; Jaeger, K. E.; Lahmann, M.; Lindhorst, T. K.; Marradi, M.; Messner, P.; Molinaro, A.; Murphy, P.
37 V.; Nativi, C.; Oscarson, S.; Penades, S.; Peri, F.; Pieters, R. J.; Renaudet, O.; Reymond, J. L.; Richichi, B.; Rojo,
38 J.; Sansone, F.; Schaffer, C.; Turnbull, W. B.; Velasco-Torrijos, T.; Vidal, S.; Vincent, S.; Wennekes, T.; Zuilhof,
39 H.; Imberty, A. *Chem. Soc. Rev.* **2013**, *42*, 4709.
40 (4) Imperiali, B. *J. Am. Chem. Soc.* **2012**, *134*, 17835.
41 (5) Kiessling, L. L.; Grim, J. C. *Chem. Soc. Rev.* **2013**, *42*, 4476.
42 (6) Wu, F.; Jin, J.; Wang, L. Y.; Sun, P. F.; Yuan, H. X.; Yang, Z. Q.; Chen, G. S.; Fan, Q. H.; Liu,
43 D. S. *ACS Appl. Mater. Interfaces* **2015**, *7*, 7351.
44 (7) Muller, C.; Despras, G.; Lindhorst, T. K. *Chem. Soc. Rev.* **2016**, *45*, 3275.
45 (8) Kitov, P. I.; Sadowska, J. M.; Mulvey, G.; Armstrong, G. D.; Ling, H.; Pannu, N. S.; Read, R. J.;
46 Bundle, D. R. *Nature* **2000**, *403*, 669.
47 (9) Fan, E. K.; Zhang, Z. S.; Minke, W. E.; Hou, Z.; Verlinde, C.; Hol, W. G. J. *J. Am. Chem. Soc.*
48 **2000**, *122*, 2663.
49 (10) Illescas, B. M. R., R.; Delgado, R.; Martín, N. *J. Am. Chem. Soc.* **2017**, *139*, 6018.
50 (11) Branson, T. R.; McAllister, T. E.; Garcia-Hartjes, J.; Fascione, M. A.; Ross, J. F.; Warriner, S. L.;
51 Wennekes, T.; Zuilhof, H.; Turnbull, W. B. *Angew. Chem. Int. Ed.* **2014**, *53*, 8323.
52 (12) Marradi, M.; Chiodo, F.; Garcia, I.; Penades, S. *Chem. Soc. Rev.* **2013**, *42*, 4728.
53 (13) Ribeiro-Viana, R.; Sanchez-Navarro, M.; Luczkowiak, J.; Koeppe, J. R.; Delgado, R.; Rojo, J.;
54 Davis, B. G. *Nat. Commun.* **2012**, *3*.
55 (14) Munoz, A.; Sigwalt, D.; Illescas, B. M.; Luczkowiak, J.; Rodriguez-Perez, L.; Nierengarten, I.;
56 Holler, M.; Remy, J. S.; Buffet, K.; Vincent, S. P.; Rojo, J.; Delgado, R.; Nierengarten, J. F.; Martin, N. *Nat. Chem.*
57 **2016**, *8*, 50.
58
59
60

- 1
2
3
4
5 (15) Geijtenbeek, T. B.; Kwon, D. S.; Torensma, R.; van Vliet, S. J.; van Duijnhoven, G. C.; Middel,
6 J.; Cornelissen, I. L.; Nottet, H. S.; KewalRamani, V. N.; Littman, D. R.; Figdor, C. G.; van Kooyk, Y. *Cell* **2000**,
7 *100*, 587.
- 8 (16) Geijtenbeek, T. B.; Torensma, R.; van Vliet, S. J.; van Duijnhoven, G. C.; Adema, G. J.; van
9 Kooyk, Y.; Figdor, C. G. *Cell* **2000**, *100*, 575.
- 10 (17) Feinberg, H.; Mitchell, D. A.; Drickamer, K.; Weis, W. I. *Science* **2001**, *294*, 2163.
- 11 (18) Pohlmann, S.; Baribaud, F.; Lee, B.; Leslie, G. J.; Sanchez, M. D.; Hiebenthal-Millow, K.; Munch,
12 J.; Kirchhoff, F.; Doms, R. W. *J. Virol.* **2001**, *75*, 4664.
- 13 (19) Kwon, D. S.; Gregorio, G.; Bitton, N.; Hendrickson, W. A.; Littman, D. R. *Immunity* **2002**, *16*,
14 135.
- 15 (20) Tabarani, G.; Thepaut, M.; Stroebel, D.; Ebel, C.; Vives, C.; Vachette, P.; Durand, D.; Fieschi, F.
16 *J. Biol. Chem.* **2009**, *284*, 21229.
- 17 (21) Pohlmann, S.; Soilleux, E. J.; Baribaud, F.; Leslie, G. J.; Morris, L. S.; Trowsdale, J.; Lee, B.;
18 Coleman, N.; Doms, R. W. *Proc. Natl. Acad. Sci. U.S.A.* **2001**, *98*, 2670.
- 19 (22) Wu, L.; KewalRamani, V. N. *Nat. Rev. Immunol.* **2006**, *6*, 859.
- 20 (23) Chung, N. P. Y.; Breun, S. K. J.; Bashirova, A.; Baumann, J. G.; Martin, T. D.; Karamchandani,
21 J. M.; Rausch, J. W.; Le Grice, S. F. J.; Wu, L.; Carrington, M.; KewalRamani, V. N. *J. Biol. Chem.* **2010**, *285*,
22 2100.
- 23 (24) Guo, Y.; Feinberg, H.; Conroy, E.; Mitchell, D. A.; Alvarez, R.; Blixt, O.; Taylor, M. E.; Weis,
24 W. I.; Drickamer, K. *Nat. Struct. Mol. Biol.* **2004**, *11*, 591.
- 25 (25) Feinberg, H.; Guo, Y.; Mitchell, D. A.; Drickamer, K.; Weis, W. I. *J. Biol. Chem.* **2005**, *280*,
26 1327.
- 27 (26) Davis, C. W.; Nguyen, H. Y.; Hanna, S. L.; Sanchez, M. D.; Doms, R. W.; Pierson, T. C. *J. Virol.*
28 **2006**, *80*, 1290.
- 29 (27) Menon, S.; Rosenberg, K.; Graham, S. A.; Ward, E. M.; Taylor, M. E.; Drickamer, K.; Leckband,
30 D. E. *Proc. Natl. Acad. Sci. U.S.A.* **2009**, *106*, 11524.
- 31 (28) Diehl, C.; Engstrom, O.; Delaine, T.; Hakansson, M.; Genheden, S.; Modig, K.; Leffler, H.; Ryde,
32 U.; Nilsson, U. J.; Akke, M. *J. Am. Chem. Soc.* **2010**, *132*, 14577.
- 33 (29) Holla, A.; Skerra, A. *Protein Eng. Des. Select.* **2011**, *24*, 659.
- 34 (30) Linman, M. J.; Taylor, J. D.; Yu, H.; Chen, X.; Cheng, Q. *Anal. Chem.* **2008**, *80*, 4007.
- 35 (31) Bruchez, M.; Moronne, M.; Gin, P.; Weiss, S.; Alivisatos, A. P. *Science* **1998**, *281*, 2013.
- 36 (32) Chan, W. C. W.; Nie, S. M. *Science* **1998**, *281*, 2016.
- 37 (33) Michalet, X.; Pinaud, F. F.; Bentolila, L. A.; Tsay, J. M.; Doose, S.; Li, J. J.; Sundaresan, G.; Wu,
38 A. M.; Gambhir, S. S.; Weiss, S. *Science* **2005**, *307*, 538.
- 39 (34) Medintz, I. L.; Clapp, A. R.; Mattoussi, H.; Goldman, E. R.; Fisher, B.; Mauro, J. M. *Nat. Mater.*
40 **2003**, *2*, 630.
- 41 (35) Zhou, D. *Biochem. Soc. Trans.* **2012**, *40*, 635.
- 42 (36) Wegner, K. D.; Hildebrandt, N. *Chem. Soc. Rev.* **2015**, *44*, 4792.
- 43 (37) Hildebrandt, N.; Spillmann, C. M.; Algar, W. R.; Pons, T.; Stewart, M. H.; Oh, E.; Susumu, K.;
44 Diaz, S. A.; Delehanty, J. B.; Medintz, I. L. *Chem. Rev.* **2017**, *117*, 536.
- 45 (38) Chinen, A. B.; Guan, C. M.; Ferrer, J. R.; Barnaby, S. N.; Merkel, T. J.; Mirkin, C. A. *Chem. Rev.*
46 **2015**, *115*, 10530.
- 47 (39) Zhang, C. Y.; Yeh, H. C.; Kuroki, M. T.; Wang, T. H. *Nat. Mater.* **2005**, *4*, 826.
- 48 (40) Zhou, D. J.; Bruckbauer, A.; Abell, C.; Klenerman, D.; Kang, D. J. *Adv. Mater.* **2005**, *17*, 1243.
- 49 (41) Somers, R. C.; Bawendi, M. G.; Nocera, D. G. *Chem. Soc. Rev.* **2007**, *36*, 579.
- 50 (42) Howarth, M.; Liu, W.; Puthenveetil, S.; Zheng, Y.; Marshall, L. F.; Schmidt, M. M.; Wittrup, K.
51 D.; Bawendi, M. G.; Ting, A. Y. *Nat. Methods* **2008**, *5*, 397.
- 52 (43) Zhang, H.; Zhou, D. *Chem. Commun.* **2012**, *48*, 5097.
- 53 (44) Benito-Alifonso, D.; Tremel, S.; Hou, B.; Lockyear, H.; Mantell, J.; Fermin, D. J.; Verkade, P.;
54 Berry, M.; Galan, M. C. *Angew. Chem. Int. Ed.* **2014**, *53*, 810.
- 55 (45) Lee, J.; Brennan, M. B.; Wilton, R.; Rowland, C. E.; Rozhkova, E. A.; Forrester, S.; Hannah, D.
56 C.; Carlson, J.; Shevchenko, E. V.; Schabacker, D. S.; Schaller, R. D. *Nano Lett.* **2015**, *15*, 7161.
- 57 (46) Wang, Q.; Liu, Y.; Ke, Y.; Yan, H. *Angew. Chem. Int. Ed.* **2008**, *47*, 316.
- 58
59
60

- 1
2
3
4
5 (47) Guo, Y.; Sakonsinsiri, C.; Nehlmeier, I.; Fascione, M. A.; Zhang, H.; Wang, W.; Poehlmann, S.;
6 Turnbull, W. B.; Zhou, D. *Angew. Chem. Int. Ed.* **2016**, *55*, 4738.
- 7 (48) Susumu, K.; Uyeda, H. T.; Medintz, I. L.; Pons, T.; Delehanty, J. B.; Mattoussi, H. *J. Am. Chem.*
8 *Soc.* **2007**, *129*, 13987.
- 9 (49) Aldeek, F.; Hawkins, D.; Palomo, V.; Safi, M.; Palui, G.; Dawson, P. E.; Alabugin, I.; Mattoussi,
10 H. *J. Am. Chem. Soc.* **2015**, *137*, 2704.
- 11 (50) Mei, B. C.; Susumu, K.; Medintz, I. L.; Mattoussi, H. *Nat. Protoc.* **2009**, *4*, 412.
- 12 (51) Song, L.; Ho, V. H. B.; Chen, C.; Yang, Z. Q.; Liu, D. S.; Chen, R. J.; Zhou, D. *J. Adv. Healthcare*
13 *Mater.* **2013**, *2*, 275.
- 14 (52) Ma, L.; Tu, C. L.; Le, P.; Chitoor, S.; Lim, S. J.; Zahid, M. U.; Teng, K. W.; Ge, P. H.; Selvin, P.
15 R.; Smith, A. M. *J. Am. Chem. Soc.* **2016**, *138*, 3382.
- 16 (53) Liu, D.; Snee, P. T. *ACS Nano* **2011**, *5*, 546.
- 17 (54) Liu, W. H.; Greytak, A. B.; Lee, J.; Wong, C. R.; Park, J.; Marshall, L. F.; Jiang, W.; Curtin, P.
18 N.; Ting, A. Y.; Nocera, D. G.; Fukumura, D.; Jain, R. K.; Bawendi, M. G. *J. Am. Chem. Soc.* **2010**, *132*, 472.
- 19 (55) Muro, E.; Pons, T.; Lequeux, N.; Fragola, A.; Sanson, N.; Lenkei, Z.; Dubertret, B. *J. Am. Chem.*
20 *Soc.* **2010**, *132*, 4556.
- 21 (56) Kong, L.; Wilson, I. A.; Kwong, P. D. *Proteins* **2015**, *83*, 590.
- 22 (57) Stewart-Jones, G. B. E.; Soto, C.; Lemmin, T.; Chuang, G. Y.; Druz, A.; Kong, R.; Thomas, P.
23 V.; Wagh, K.; Zhou, T. Q.; Behrens, A. J.; Bylund, T.; Choi, C. W.; Davison, J. R.; Georgiev, I. S.; Joyce, M. G.;
24 Do Kwon, Y.; Pancera, M.; Taft, J.; Yang, Y. P.; Zhang, B. S.; Shivatare, S. S.; Shivatare, V. S.; Lee, C. C. D.;
25 Wu, C. Y.; Bewley, C. A.; Burton, D. R.; Koff, W. C.; Connors, M.; Crispin, M.; Baxa, U.; Korber, B. T.; Wong,
26 C. H.; Mascola, J. R.; Kwong, P. D. *Cell* **2016**, *165*, 813.
- 27 (58) Zhang, H.; Li, S.; Lu, R.; Yu, A. *ACS Appl. Mater. Interfaces* **2015**, *7*, 21868.
- 28 (59) Zhang, H.; Feng, G.; Guo, Y.; Zhou, D. *Nanoscale* **2013**, *5*, 10307.
- 29 (60) Lee, J. H.; Ozorowski, G.; Ward, A. B. *Science* **2016**, *351*, 1043.
- 30 (61) Hondow, N.; Brydson, R.; Wang, P.; Holton, M. D.; Brown, M. R.; Rees, P.; Summers, H. D.;
31 Brown, A. *J. Nanopart. Res.* **2012**, *14*.
- 32 (62) Mitchell, G. P.; Mirkin, C. A.; Letsinger, R. L. *J. Am. Chem. Soc.* **1999**, *121*, 8122.
- 33 (63) Samanta, A.; Zhou, Y.; Zou, S.; Yan, H.; Liu, Y. *Nano Lett.* **2014**, *14*, 5052.
- 34 (64) Kong, Y. F.; Chen, J.; Fang, H. W.; Heath, G.; Wo, Y.; Wang, W. L.; Li, Y. X.; Guo, Y.; Evans,
35 S. D.; Chen, S. Y.; Zhou, D. *J. Chem. Mater.* **2016**, *28*, 3041.
- 36
37
38
39
40
41
42
43
44
45
46
47
48
49
50
51
52
53
54
55
56
57
58
59
60

Table of Content graph

